AIAA JOURNAL
Vol. 37, No. 6, June 1999

Planar Doppler Velocimetry: Three-Component Velocimetry in Supersonic Jets

Pamela S. Clancy,* Mo Samimy,† and William R. Erskine‡
Ohio State University, Columbus, Ohio 43210-1272

A three-component planar Doppler velocimetry system was developed and used to make mean and instantaneous velocity measurements in a Mach 2 axisymmetric freejet. The mean measurements were in good agreement with reference laser Doppler velocimetry measurements taken in the same flowfield, whereas the instantaneous measurements were in fair agreement and indicated areas that required improvement. A detailed uncertainty analysis provided further insight into the performance of the planar Doppler velocimetry system. The calibration of the splitter/recombiner imaging system using flatfield images was improved. Speckle image noise was found to be the largest source of error affecting the turbulence results, and so digital filtering techniques were investigated and employed.

Nomenclature

B, B_i	= bias limit and ith term contributing to the bias limit
$\boldsymbol{o}$	= unit vector pointing in the propagation direction of the laser light
p_{I_2}, p_{N_2}	= partial pressure of iodine and nitrogen, torr
S, S_i	= precision limit and ith term contributing to the precision limit
$\bar{S}$	= contribution of the precision limit to the mean uncertainty
$\boldsymbol{s}$	= unit vector pointing in the direction of observation
$\boldsymbol{V}$	= particle velocity
x, y, z	= system coordinates as defined in the text
α, β, γ	= viewing angle of Doppler shift measuring systems $(DSMS)_A$, $DSMS_B$, and $DSMS_C$
Δf_d	= Doppler shift in frequency
λ	= laser light wavelength
σ	= standard deviation
ω_v	= instantaneous velocity uncertainty
$\bar{\omega}_v$	= mean velocity uncertainty
$\omega_{\Delta f_d}$	= instantaneous Doppler shift uncertainty
$\bar{\omega}_{\Delta f_d}$	= mean Doppler shift uncertainty

Introduction

PLANAR Doppler velocimetry (PDV) is a powerful nonintrusive planar optical velocimetry technique that utilizes a molecular filter as a frequency discriminator. Researchers have been using molecular filters for a number of years in various capacities.[1–3] The type of information that can be obtained from the scattering signal depends on the regime into which the scattering falls. The PDV configuration here is based on measurements of Rayleigh–Mie scattered light. For this regime, the line shape of the incident light is preserved, which is characteristic of Mie scattering. As a result, solely the Doppler shift, hence velocity, can be resolved. The fundamental basis of PDV and Doppler global velocimetry (DGV) are the same. Techniques, whether termed PDV or DGV, may vary in the type of filter broadening, type of filter vapor, and/or type of laser used. An important feature of the work here, which distinguishes it from the DGV work reported in the literature, is that a pressure-broadened filter, which increases the dynamic range of the technique, was used.

In PDV, the Doppler-shifted frequency of light scattered by particles in the flowfield passing through a laser sheet formed using a narrow linewidth laser is measured. Using a short-duration pulsed Nd:YAG laser, the velocity measurements can be considered instantaneous. The scattering medium can be injected seed particles and/or naturally occurring particles in the flowfield. The Doppler shift Δf_d of the scattered light is given by the Doppler shift equation of Yeh and Cummins[4]:

$$\Delta f_d = \frac{(\boldsymbol{s} - \boldsymbol{o})}{\lambda} \cdot \boldsymbol{V} \tag{1}$$

The primary components of the PDV experiment include the seed particles, laser sheet, molecular filter, and splitter/recombiner systems. It is the use of the molecular filter that enables the planar capabilities of PDV. In PDV, the Doppler-shifted frequency is determined by comparing the intensities of two images of the same flowfield. For one of the images, the scattered light will have been attenuated by an optical filter before being recorded. The frequency dependence of the optical filter attenuation is used to extract the Doppler shift.

The PDV technique has been investigated and refined over the years. Komine et al.[5] demonstrated the feasibility of the PDV technique but did not quantify their results. Meyers et al.[6] demonstrated multiple-component velocity measumements in a low-speed flowfield. Elliott et al.[7] used the technique to measure one component of velocity in compressible mixing layers. The technique was advanced to resolve two components of velocity in a supersonic boundary layer by Arnette et al.[8] and in a supersonic freejet by Clancy and Samimy.[9] Smith et al.[10] implemented the idea of a splitter/recombiner system, which reduced the cost of PDV experimentation, and first recognized the problem of speckle noise. McKenzie[11,12] documented the measurement capabilities of PDV and presented a detailed description of possible error sources. Clancy and Samimy[9] and Clancy et al.[13] improved the technique by incorporating a frequency-monitoring system into the two-component measurements and identifying methods to improve PDV data collection procedures. This paper extends the measurement technique to three components. The velocity measurements were made in a supersonic jet. Two different three-component PDV configurations are presented with associated experimental results and uncertainty analysis.

Experimental Setup

The baseline flowfield was an ideally expanded Mach 2 freejet. The flow was unheated, and the Reynolds number based on the

Presented as Paper 98-0506 at the AIAA 36th Aerospace Sciences Meeting, Reno, NV, Jan. 12–15, 1998; received Feb. 28, 1998; revision received Oct. 26, 1998; accepted for publication Nov. 6, 1998.

*Graduate Student, Department of Mechanical Engineering; currently Senior Member of the Technical Staff, Fluid and Thermophysics Department, TRW Space and Electronics Group, Redondo Beach, CA 90278. Senior Member AIAA.

†Professor and Associate Chair, Department of Mechanical Engineering. Associate Fellow AIAA.

‡Graduate Student, Department of Mechanical Engineering. Member AIAA.

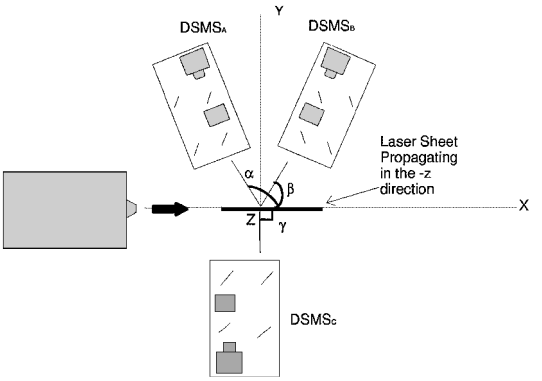

Fig. 1 Plan view of the three-component SW-PDV system.

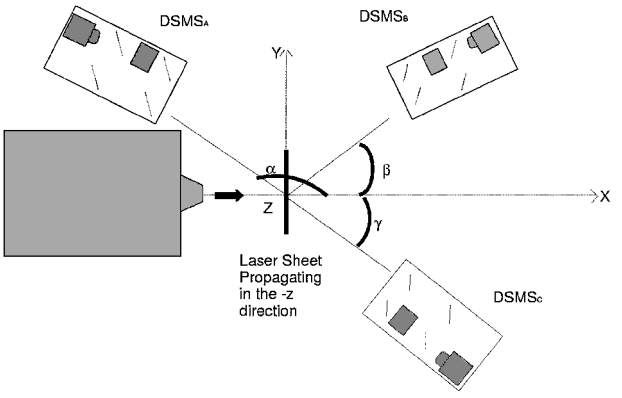

Fig. 2 Plan view of the three-component CS-PDV system.

jet exit diameter of 19 mm was 2.1×10^6. To resolve three components of instantaneous velocity, three Doppler shift measuring systems (DSMSs), each viewing the measurement region from a different viewing angle, were required. The three-component streamwise PDV (SW-PDV) measurement region was located along the centerline of the jet and extended from 5.8 to 7.8 jet diameters downstream of the jet exit. As shown in Fig. 1, $DSMS_A$, $DSMS_B$, and $DSMS_C$ were located in the x–y plane at viewing angles of $\alpha = 121$, $\beta = 63$, and $\gamma = -90$ deg, respectively, relative to the x axis. The three-component cross-stream PDV (CS-PDV) measurement volume was located 6 jet diameters downstream of the jet exit. $DSMS_A$, $DSMS_B$, and $DSMS_C$ were located in the x–y plane at viewing angles of $\alpha = 129$, $\beta = 32$, and $\gamma = -37$ deg relative to the x axis (Fig. 2).

The experiments were conducted at the Aeronautical and Astronautical Research Laboratory of Ohio State University. Dry and compressed air was stored in two tanks with a total capacity of 42.5 m^3 at 17 MPa. Data collection commenced when the stagnation temperature had settled. The stagnation pressure was maintained within 2% of the desired pressure. The laser was an injection-seeded, Nd:YAG Quanta Ray laser operating at a frequency-doubled wavelength of 532 nm. The laser had a 9-ns pulse duration, 10-Hz repetition rate, and 100-MHz approximate linewidth. The laser sheet was formed from the centermost portion of the laser beam and was verified to have a consistent frequency content.[9] Variations in frequency across the laser sheet will introduce errors when the filtered-to-unfiltered intensity ratio is converted to an equivalent Doppler shift. One can either take into account frequency variations or remove frequency variations by limiting the portion of the laser beam that is used. The images were collected on Princeton Instruments, Inc., cooled, intensified, 14-bit, charge-coupled device (ICCD) cameras. A Tamaron SPF2BB 90-mm camera lens, with an indicated f number of approximately 6.8, was used with each camera. All images were collected by operating the camera in a bin-by-2 mode, resulting in images consisting of 288×192 superpixels. For the SW-PDV and CS-PDV configurations, the superpixel object size corresponded to approximately 480 and 500 μm in the flowfield, respectively.

Table 1 Vapor component partial pressure for each filter used in the three-component SW- and CS-PDV systems in terms of torr as p_{I_2}/p_{N_2}

System	SW-PDV	CS-PDV
$DSMS_A$	4.28/41.0	3.05/40.0
$DSMS_B$	4.28/41.0	4.28/41.0
$DSMS_C$	3.05/30.0	4.28/41.0
FMON	5.05/22.5	5.05/40.0

Condensed water particles and condensed acetone particles primarily marked the jet shear layer and jet center region, respectively. The ambient air surrounding the jet was not seeded for either the PDV or laser Doppler velocimetry (LDV) reference measurements. The condensed water particles formed when warm moist ambient air mixed with the cold and dry jet flow. The condensed acetone particles were formed by vaporizing acetone from a pressurized tank into the primary flow.[9,14] The amount of acetone seeding was estimated to be less than 0.4% of the airflow by weight.[9,14] The diameter of both types of particles was estimated to be on the order of 50 nm (Refs. 9 and 15), small enough to follow the high-speed flow.[16] The scattering of the coherent light from these particles produced speckle noise. To reduce the effect of speckle noise, all of the raw images were passed through a short-space, low-pass filter.[9,17]

Each DSMS consisted of a splitter/recombiner system,[9] a camera, and a molecular filter.[7] The filtered and unfiltered images were collected side-by-side on one camera.[9,10,12,13,18] The method of Clancy and Samimy[9] was used to obtain subpixel image registration. Each filter was 10 cm in length and 10 cm in diameter. The amount of iodine and nitrogen contained in the filter was varied by trial and error until the desired transmission profile for the expected flow Doppler shifts was obtained. The main features of the filter cell described by Elliott et al.[7] was used. The partial pressure of the iodine is extremely sensitive to the temperature of the coldest portion of the cell, typically a cold finger whose temperature is controlled by a water jacket, but is not sensitive to the temperature of the main part of the cell.[14] Once the desired partial pressure of iodine reached equilibrium, a stopcock was used to trap the desired amount of vapor in the main part of the cell. Subsequent use of the cell merely required the temperature of the main part of the cell to be raised until all of the crystals in the main part of the cell were in a vapor state. The filter cell temperature, set by using an Ohmite variable transformer and heat tape, was maintained within 2 K of the desired temperature. The partial pressure of iodine and nitrogen of each filter is listed in Table 1, in terms of torr, as p_{I_2}/p_{N_2}. Both systems included a frequency monitoring (FMON) system, and the associated FMON filter components are also listed in Table 1. Although maximum resolution is desired for the FMON filter, it is also necessary to have the slope of the profile in the vicinity of the frequency set point. Thus, in comparison with the other filters, the FMON-filter-increased amount of iodine shifts the intercept, and the decreased amount of nitrogen maintains as much of the slope as possible. The absorption line of iodine at 18788.4 cm^{-1} was used in these experiments.

Flatfield images were obtained to properly calibrate the DSMS for camera gain variations, for optical variations across each image, and for the polarization dependence quality of the beam splitters. The method used for previous two-component PDV systems[9] was used to calculate the flatfield images for the SW-PDV system. This method was believed to be a source of error in the SW-PDV measurements. An improved method was developed and used in obtaining the flatfield images for the three-component CS-PDV data. The improved method involved taking the calibration images with the laser unseeded, which removed the dependence of the flatfield images on flow velocity, and taking the images at four different laser intensities. For each pixel in the filtered region, the intensity at the corresponding pixel in the unfiltered region was known for each of the four distinct intensity levels. Using the linear quality of the cameras,[8] a line was drawn through the filtered and unfiltered intensity data points. In general, the intercept is small, and the image composed of the slope values constitutes the flatfield image. Additional details of this technique can be found in Refs. 14 and 17. The flatfield and intercept images are very useful representations of the quality of the data and image registration accuracy.[14,17]

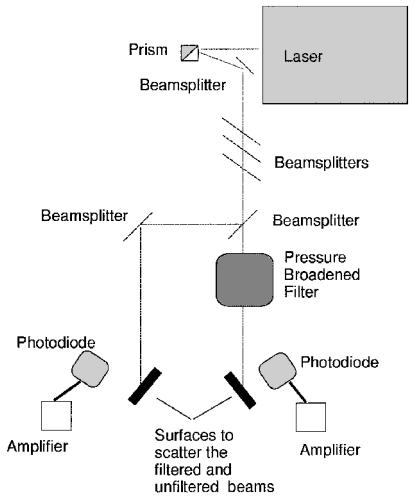

Fig. 3 Schematic of the FMON system used with the CS-PDV system.

FMON System

The laser frequency fluctuates and drifts. The pulse-to-pulse variations in the laser frequency are random fluctuations in time about a mean, and that mean may slowly drift in time. Because the measured Doppler shift is relative to the laser frequency, any variation of laser frequency would produce an error in the measured Doppler shift and resulting velocity calculations. Systems to monitor the laser frequency have been proposed and/or implemented by various researchers.[7,10,11,13,14,19] Two slightly different FMON systems were used for the CS-PDV and SW-PDV configurations.[14] The version used for the CS-PDV configuration is presented in Fig. 3. It consisted of a pressure-broadened filter, two ET 2000 photodetectors, two high-impedance amplifiers, and an analog-to-digital board operating from a personal computer. The combination of the high-impedance amplifiers and the photodiodes resulted in a peak hold-type signal. Data collection of the signals was synchronized with the triggering of the camera images. Reference 14 describes in more detail possible configurations and their advantages and drawbacks. Although the FMON system appears to account effectively for laser drift, the instantaneous accuracy of the system is yet to be determined.

Reference LDV

To investigate the accuracy of the PDV velocity results, a set of LDV velocity measurements was obtained in the same flowfield. LDV, being an established velocimetry technique, allowed the LDV data to be used as a reference for the PDV data. The LDV data obtained with a TSI, Inc., two-component, fiber-optic-based system are discussed in more detail in Ref. 9. Inasmuch as LDV is a pointwise measurement technique, mean and turbulence measurements of the x and z components of velocity were made only along the vertical centerline of the jet, at a location of 6 jet diameters downstream of the jet exit.

Experimental Results

Three-Component SW-PDV Results

To obtain mean and turbulence results in a Mach 2 jet, 12 velocity runs were performed, and 50 velocity images were obtained for each run. Five of these runs were excluded because the FMON showed fluctuations exceeding 25 MHz (Ref. 14). The frequency fluctuation of the remaining runs was approximately ± 20 MHz. A 10-MHz frequency fluctuation, which is specified by the laser manufacturer, was measured with the FMON system when the jet was not running.

In Fig. 4, the left-hand column shows the unfiltered image and the right-hand column shows the filtered image for each DSMS. Variations in the intensity of the unfiltered images correspond to optical variations in the DSMS and density variations in the flowfield. Variations in the intensity of the filtered images correspond to the combination of DSMS optical variations and transmission variations due to the Doppler-shifted frequency. Because of the orientation of the

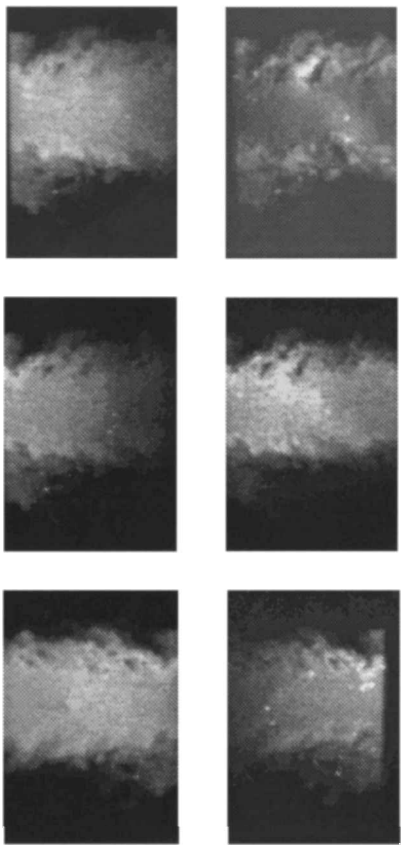

Fig. 4 Velocity image from top to bottom for $DSMS_A$, $DSMS_B$, and $DSMS_C$ for one instant in time; the left-hand column shows unfiltered images, and the right-hand column shows filtered images.

DSMSs, the flowfield is traveling from right to left in the images of $DSMS_A$ and $DSMS_B$ and from left to right in the images of $DSMS_C$. The images alone provide insight into the flowfield. For example, for $DSMS_A$, the Doppler-shifted scattering from particles moving with positive axial velocity is in the direction of the well of the filter profile. Thus, the jet center region, which is of greater axial velocity, is darker than the shear layer. In addition, the diagonal feature in the filtered images is believed to be associated with a weak shock cell structure in the jet.

Only images that had a minimal number of saturated pixels were used in the velocity and flatfield calculations. The final data set consisted of 251 velocity images. Furthermore, any region that was considered to be scattering from a large particle, or was below a signal-to-noise ratio (SNR) of 1.5, was not included in the velocity or turbulence calculations. The mean velocity, at any given point, was calculated by taking the average of the instantaneous velocities.[9,10] The average velocity vector field, composed of the x and z components of velocity, is presented in Fig. 5. The growth of the shear layer, as a function of downstream distance, is captured clearly in Fig. 5.

The top panel of Fig. 6 compares the mean SW-PDV velocity measurements, both with and without the incorporation of the FMON measurements, with the reference LDV measurements at a location 6 jet diameters downstream from the jet exit. All of the velocities were normalized by the centerline x component of velocity, approximately 500 m/s, and the distances were normalized by the jet diameter, 19 mm. The shapes of the PDV velocity profiles consistently match the shapes of the LDV profiles. The slight deviation in the x component of velocity was believed to be related to errors associated with the flatfield images. The flatfield images were obtained from calibration images taken of the flowfield with the laser frequency set to correspond to approximately full transmission of the molecular filters. However, given the range of positive and negative Doppler shifts realized in this configuration, it was difficult to set the laser frequency such that the flatfield images would be insensitive to velocity information. The middle panel of Fig. 6 compares the SW-PDV y component of velocity, with and without FMON,

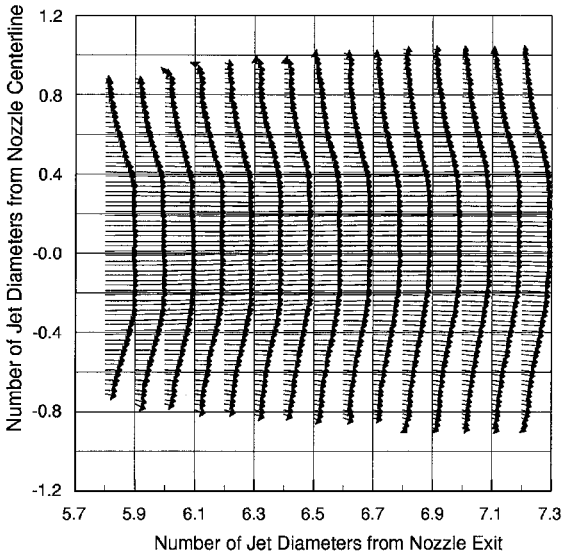

Fig. 5 SW-PDV mean streamwise velocity vector field.

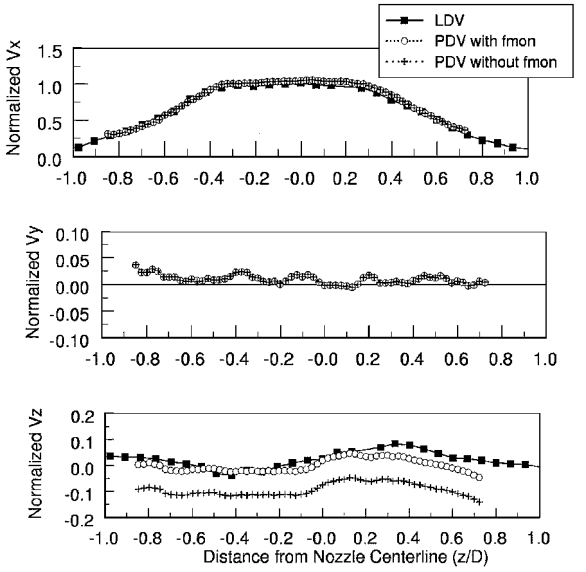

Fig. 6 Mean velocity results of SW-PDV, with and without FMON corrections, compared with LDV measurements.

with the expected level of 0 m/s. The y component of velocity was not measured with LDV. The magnitude of the SW-PDV y component of velocity is small, as is expected. The bottom panel of Fig. 6 compares the mean z component of velocity, both with and without the FMON corrections. Without the FMON corrections, a bias error affects the z component of velocity. The incorporation of the FMON measurements removes this bias. The propagation of the frequency drift in only one component is an artifact of the resulting system of equations. When the DSMSs are constrained to the x–y plane, only the z component of velocity is a function of the Doppler shift from one viewing direction. The other components are a function of the difference between two Doppler shifts, rendering the reference frequency irrelevant.[17]

In Fig. 6, the SW-PDV and LDV Vz profiles do not exactly match. One possible explanation stems from the difference in the seeding methods used for the two techniques. The LDV measurements were based on oil particles that would mark the entire jet flow. The PDV measurements were based on condensed water and acetone particles, the existence of which depends on the details of the flowfield. For example, the PDV measurements in the shear layer are based on the instantaneous flowfields in which the temperature was low enough and the amount of entrained moisture was large enough to produce a detectable scattered signal. This seeding method is also why the velocity and turbulence profiles do not continue through the shear

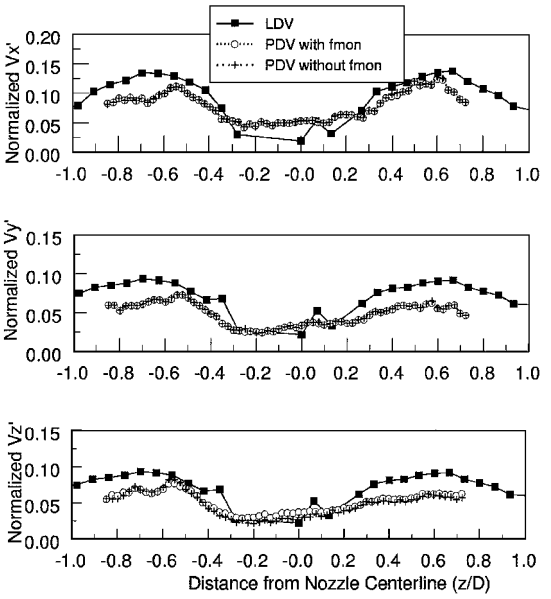

Fig. 7 Comparison of SW-PDV turbulence results, with and without the incorporation of FMON corrections, with the LDV measurements.

layer to the ambient. The seeding technique was useful in developing the PDV techniques; however, for detailed measurements of the jet statistics, the jet flow and ambient air surrounding the jet should be seeded.

Figure 7 compares the LDV and PDV turbulence intensities. Three LDV measured points in the core region of the jet that were noise dominated have been removed.[14] The incorporation of the FMON information does not significantly influence the turbulence intensities. For all of the components, the SW-PDV turbulence is slightly lower than the LDV turbulence. Part of the reason is the low-pass filtering of the images that was performed to reduce the adverse effect of speckle noise.[14] However, it is not evident why the SW-PDV turbulence intensity is lower than the LDV measurements even when the low-pass filter has not been applied. The convergence of the SW-PDV measured turbulence level with an increased number of data samples was investigated.[14] It was shown that the turbulence level settled out after about 100–150 PDV images were included in the statistics. This is also true for the CS-PDV case.

Three-Component CS-PDV Results

Six velocity runs were performed, and 50 velocity images were obtained for each run. The final data set consisted of 296 velocity images, which intersected the jet flow in a cross-stream plane. Note that planar velocimetry techniques such as traditional particle image velocimetry, which depend on particle transit time, cannot obtain velocity measurements on a cross-stream plane. Stereo particle image velocimetry, however, has been used to make three-component measurements on a cross-stream plane but uses a much thicker laser sheet, which degrades the spatial resolution of the measurements.[20] A FMON system was used to calculate the pulse-to-pulse laser frequency. The frequency fluctuation was approximately ± 18 MHz for all of the runs.

Because of the CS-PDV configuration, speckle was seen to degrade significantly the accuracy of the y component of velocity. Speckle noise in relation to PDV has been mentioned by various researchers.[9,10,12,14,17] Fundamentally, the speckle pattern in the image is produced by the phase variation of the light waves produced by the scattered medium. As the phase variations over the scattered region increase, the contrast in the speckle pattern increases. For phase variations larger than the wavelength of light, a saturation limit is reached,[21–23] and the speckle noise becomes primarily a function of the optics.[12,24–26] Both McKenzie[12] and Arsenault and April[24] present formulations to approximate the speckle noise.

To reduce the error associated with speckle, several noise reduction filter techniques were investigated.[27–29] To remove a multiplicative noise, such as speckle, linear filters are applied to the log of the

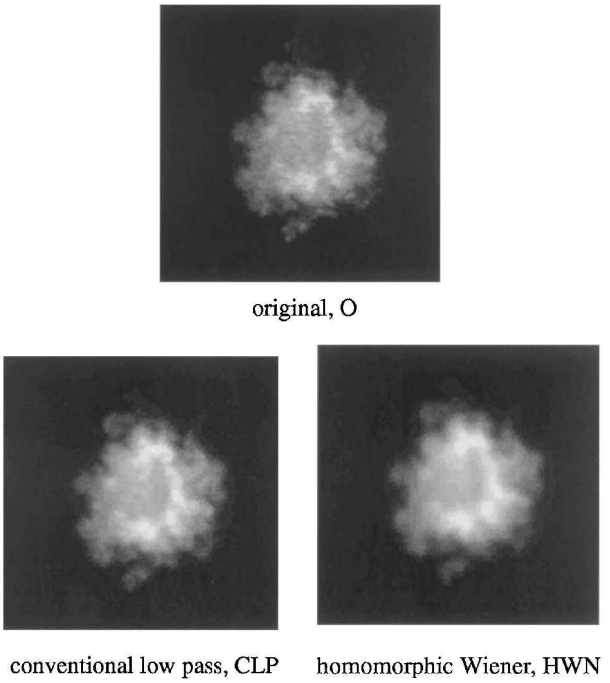

Fig. 8 Example results of applying a conventional low-pass filter and a homomorphic Wiener filter to the original unfiltered scattered image.

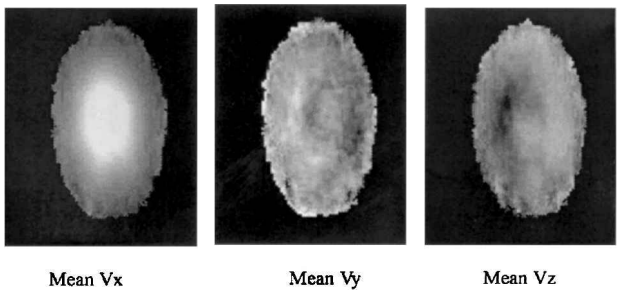

Fig. 9 Three-component CS-PDV planar mean velocity maps; relatively brighter regions indicate greater relative velocities.

intensity, and then the antilog of the filtered data is taken to recover the intensity. A conventional filter applied in this manner is denoted a *homomorphic filter*. Typically, Wiener filters and filters applied on a short-space basis are most effective.

Comparison of a short-space, 3×3 pixel window, low-pass filter with weighted coefficients and a short-space, 4×4 pixel window, homomorphic Wiener filter was presented by Clancy et al.[17] Figure 8 shows an original unfiltered scattered image, the results of a conventional low-pass filter, and the results of a homomorphic Wiener filter applied to the original image. The size of the short-space window and the details of the digital filtering affect the resultant degradation in spatial resolution and measured frequency content of the turbulence. A detailed analysis of each filter is beyond the scope of these preliminary attempts; however, in Fig. 8 the spottiness of the original image is removed more effectively with the homomorphic Wiener filter while the perimeter and size of the main features are preserved.

Figure 9 shows the planar velocity images, where the relatively increasing intensity corresponds to relatively increasing velocities.[17] Any region that was considered to be scattering from a large particle, or was below a SNR of 2.0, was not included in the velocity or turbulence calculations.

Figure 10 compares the mean LDV results with the CS-PDV results with and without the incorporation of FMON, indicated as with FMON and without FMON, respectively. Figure 10 also compares the results when a low-pass filter and a homomorphic Wiener filter were used to reduce speckle noise, denoted as filter LP and filter W, respectively. The shapes of CS-PDV velocity profiles consistently match the shapes of the LDV profiles. Notice that the x component of velocity matches the LDV x component of velocity

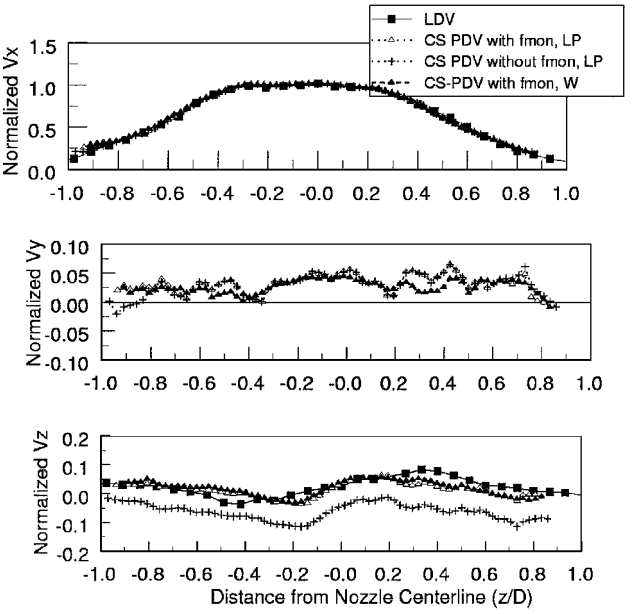

Fig. 10 Comparison of three-component mean velocity results using CS-PDV, with and without the incorporation of FMON corrections, with LDV measurements showing effect of homomorphic Wiener filter on the CS-PDV mean measurements.

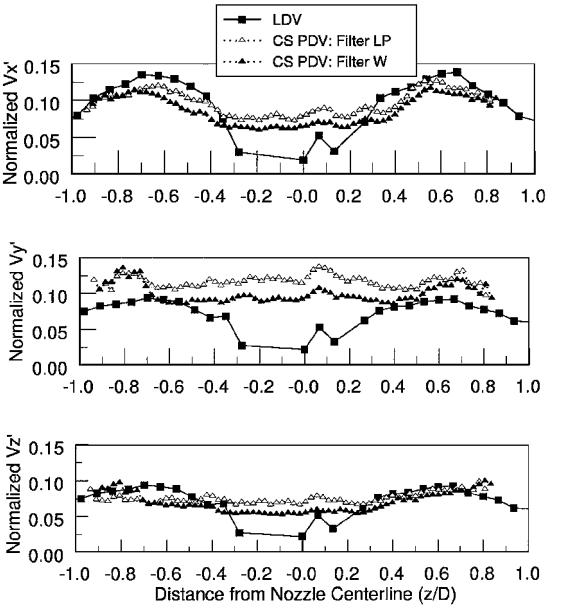

Fig. 11 Effect of homomorphic Wiener filter on the CS-PDV turbulence intensity.

very well. The slight error in the SW-PDV x component of velocity is not seen here. The velocity errors resulting from errors in determining the flatfield images were believed to be greatly reduced as a result of the improved method of determining the flatfield. As with the SW-PDV results, the middle panel of Fig. 10 compares the CS-PDV y component of velocity, with and without FMON, with a level of 0 m/s. The CS-PDV y component of velocity fluctuates more and is of larger magnitude than the SW-PDV y component of velocity. Notice that, when the homomorphic Wiener filter is used, the results are smoother. From the uncertainty analysis, it was found that the speckle image noise and PDV errors are amplified for the y component of velocity due to the cross-stream configuration. The bottom panel of Fig. 10 compares the mean z component of velocity, both with and without the incorporation of FMON. Similar to the SW-PDV results, the errors due to the uncertainty in the absolute frequency primarily affect the z component of velocity.

Figure 11 compares the LDV and CS-PDV turbulence intensities, again using a low-pass filter and the homomorphic Wiener filter.

Both sets of data incorporate the FMON corrections. However, the FMON information does not noticeably influence the results. The x component of turbulence is consistent with the LDV results. However, the y component of turbulence appears to be noise dominated, and the z component of turbulence is significantly affected by noise. The largest source of the noise was found to be speckle image noise. Notice that with the application of the homomorphic Wiener filter the turbulence intensities for the x and z component are noticeably reduced; however, the y component of turbulence remains noise dominated.

These results indicate that speckle noise is a significant challenge to the success of detailed turbulence measurements. The configuration of the PDV system also has an important impact on the quality of the results. Recall that the SW-PDV turbulence measurements were in better agreement with the LDV turbulence results (Fig. 7).

Uncertainty Analysis

The mean three-component PDV results compared very well with reference LDV measurements, whereas the turbulence measurements indicated the need for improvement. An uncertainty analysis was performed to provide additional insight into the areas that need improvement. The uncertainty analysis investigates the uncertainty in the PDV measured mean and instantaneous velocity. First, the uncertainty in the Doppler shift measurement is estimated, and then the propagation of the Doppler shift uncertainty combined with angle measurement uncertainty into the velocity measurements is estimated. In PDV, various sources of error, listed in Table 2, introduce a fixed error, or bias, into the results and others introduce a random, or precision, error. The techniques described by Kline and McClintok[30] and by Moffat[31] were used as the basis for the uncertainty analysis. The component uncertainties were based on actual data or models or were chosen from experience gained by working with the PDV system.

Doppler Shift Measurement Uncertainty

In this section the uncertainties associated with various terms are briefly discussed. Additional details are presented in Ref. 14. Tables 3 and 4 present the Doppler shift uncertainty terms for the SW-PDV and the CS-PDV systems, respectively. Because of the propagation of errors in different regions of the flowfield, the uncertainties are listed for each DSMS corresponding to a region in the jet center and shear layer. The propagation of the individual uncertainties was defined in terms of a bias limit and a precision limit. The precision limit and bias limit were combined to determine the uncertainty in the mean and instantaneous measurement of the Doppler shift. To account for the finite sample size of the results, a statistical portion of the precision limit, based on the sample size and 95% confidence level, was included in the bias limit.[14,31,32] Each of the terms are briefly discussed as follows.

The term B_1 represents the uncertainty in determining the intercept value for the molecular filter transmission profiles. This term is associated with the variation of frequency content across the laser sheet, which can be minimized by properly setting up the laser sheet. The uncertainty in determining the calibrated filter transmission profile intercept value was ± 2 MHz.

Table 2 PDV components errors

PDV component	Error source	Type of error
ICCD camera	Dark noise, readout noise, nonlinearity, photon statistical noise	Random
Laser sheet	Drift, fluctuation, nonuniform content	Fixed, random
Molecular filter	Calibration errors, conversion factor errors	Fixed
Splitter/recombiner	Flatfield image, image registration	Fixed
Particle scattering	Speckle image noise	Random
Multiple DSMS	Angle errors, Doppler shift registration	Fixed

Table 3 SW-PDV Doppler shift uncertainty[a]

	$DSMS_A$, MHz		$DSMS_B$, MHz		$DSMS_C$, MHz	
Term	JC	SL	JC	SL	JC	SL
B_1	2	2	2	2	2	2
B_2	2	6	8	16	1	2
B_3	4	4	4	4	4	4
B_4	2	2	5	9	N/A	N/A
B	5	8	10	19	5	5
S_1	2	4	13	13	2	2
S_2	10	10	10	10	10	10
S_3	25	25	80	80	20	20
S	27	27	82	82	22	22
$\bar{S}$	3	3	10	10	3	3
$\bar{\omega}_{\Delta f_d}$	6	9	14	21	6	6
$\omega_{\Delta f_d}$	27	28	83	84	23	23

[a]JC, jet center, and SL, shear layer.

Table 4 CS-PDV Doppler shift uncertainty[a]

	$DSMS_A$, MHz		$DSMS_B$, MHz		$DSMS_C$, MHz	
Term	JC	SL	JC	SL	JC	SL
B_1	2	2	2	2	2	2
B_2	1	7	3	10	2	11
B_3	0	0	4	4	3	1
B_4	N/A	N/A	2	16	3	16
B	2	7	6	19	5	20
S_1	5	9	9	8	10	9
S_2	10	10	10	10	10	10
S_3	18	18	78	78	67	67
S	21	23	80	80	68	68
$\bar{S}$	2	3	9	9	7	7
$\bar{\omega}_{\Delta f_d}$	3	8	11	21	9	21
$\omega_{\Delta f_d}$	21	24	80	82	68	71

[a]JC, jet center, and SL, shear layer.

The term B_2 represents the errors in obtaining the transmission coefficient due to errors in image registration. The uncertainty estimate was based on the gradient of intensity with respect to pixel location based on actual data and an assumed 0.3 error in pixel alignment.

The term B_3 represents the uncertainty in the measured scattered frequency resulting from uncertainties in the flatfield images. The uncertainties in the flatfield images correlate with uncertainties in the measured transmission coefficient and then propagate into the velocity calculations. The resultant Doppler shift uncertainty ranged from ± 1 to ± 4 MHz.

The term B_4 represents the uncertainty associated with errors in aligning the Doppler shift image from aligning two of the DSMSs with the third. The error in registering the Doppler shift images was modeled in a manner analogous to that of B_2, where the Doppler shift gradient was used instead of the intensity gradient. Tables 3 and 4 give the uncertainty in the Doppler shift measurement for the DSMSs that were aligned with the reference DSMS.

The term S_1 represents the uncertainties in the measured frequency due to the 1% nonlinearity of the camera reading.[9,14] This term was modeled based on the values that were typical of the data set. The uncertainty in the measured Doppler-shifted frequency resulting from camera nonlinearities ranged from ± 2 to ± 13 MHz for the SW-PDV system and was on the order of ± 10 MHz for the CS-PDV system.

The term S_2 represents the uncertainty in the instantaneous laser frequency fluctuations. The fluctuations are primarily averaged out of the mean velocity measurements but are anticipated to affect the turbulence intensity. The instantaneous capabilities of the FMON system have not been qualified. An uncertainty estimate in the FMON system's measurement of the laser frequency was taken to be approximately ± 10 MHz. This value represents the increase in the frequency fluctuation, which was measured with the FMON system when the jet was operating. Laser drift, which was corrected for with the FMON system, was not included in the uncertainty analysis.

The term S_3 represents the instantaneous uncertainty resulting from speckle image noise. The speckle SNR ranged from 2 to 4

Table 5 SW-PDV velocity uncertainty[a]

	V_x/V_c		V_y/V_c		V_z/V_c	
Uncertainty	JC	SL	JC	SL	JC	SL
$\bar{\omega}_{v,\Delta f_d}$	3	4	2	2	1	2
$\omega_{v,\Delta f_d}$	16	16	5	5	5	5
$\omega_{v,a}$	4	3	2	1	2	1
$\bar{\omega}_v$	5	4	2	2	2	2
ω_v	16	16	5	5	5	5

[a]JC, jet center, and SL, shear layer.

Table 6 CS-PDV velocity uncertainty[a]

	V_x/V_c		V_y/V_c		V_z/V_c	
Uncertainty	JC	SL	JC	SL	JC	SL
$\bar{\omega}_{v,\Delta f_d}$	2	3	2	5	1	3
$\omega_{v,\Delta f_d}$	12	12	16	17	8	8
$\omega_{v,a}$	2	1	2	1	2	1
$\bar{\omega}_v$	3	3	3	5	2	3
ω_v	12	12	16	17	8	8

[a]JC, jet center, and SL, shear layer.

for the three-component PDV systems. An uncertainty in the transmission coefficient was deduced, and the resulting Doppler shift uncertainty is listed in Tables 3 and 4. The instantaneous speckle uncertainty is quite large.

The overall mean and instantaneous Doppler shift uncertainties are presented in Tables 3 and 4. The uncertainty in the mean measured Doppler shift was less than or equal to ± 14 MHz for the jet center region and ± 21 MHz for the shear layer region for both the CS-PDV and SW-PDV systems. Notice that the uncertainty was smaller for $DSMS_A$ for both the CS-PDV and SW-PDV. The Doppler shift for $DSMS_A$ for both systems was negative, and the scattered frequency was shifted closer to the well of the transmission profile. Also, the Doppler shift for $DSMS_C$ of the SW-PDV system did not have a significant Doppler shift and showed a smaller uncertainty.

The uncertainty in the instantaneous measured Doppler shift is much larger, with the largest source of uncertainty resulting from speckle noise. Notice that the DSMSs, which, due to their viewing angle, detect large positive Doppler shifts, i.e., $DSMS_B$ and $DSMS_C$ of the CS-PDV system and $DSMS_B$ of the SW-PDV system, also show the largest uncertainty in the instantaneous Doppler shift measurement.

Velocity Uncertainty

Errors associated with viewing angle measurements and Doppler shift calculations will propagate into the final velocity calculations. Tables 5 and 6 summarize the uncertainty in the velocity for the jet center region and shear layer region. The results are presented in terms of percent centerline velocity.

In the PDV experiment, the Doppler shift equation is dependent on the viewing angle of the DSMS. The error in measuring the viewing direction from the centerline of the image to the center of the jet was assumed to be ± 1 deg. The method used to measure the angles and the estimated error in the velocity was discussed in Ref. 14. The results are presented in Tables 5 and 6.

The effect of the mean and instantaneous measured Doppler shift uncertainties on the resolved velocity components was modeled as described in Ref. 14. The 2σ uncertainties on the x, y, and z component of mean and instantaneous velocity, $\bar{\omega}_v$ and ω_v, respectively, for each case are presented in Tables 5 and 6.

In reviewing the results of the uncertainty analysis on the mean and instantaneous components of velocity, a few trends are apparent. First, the mean velocities were quite accurate. Note that the mean uncertainties are less than 5% of the jet centerline velocity for both PDV configurations. The uncertainty analysis presented here closely approximates the difference between the LDV and the PDV results.[17] Differences between the PDV and LDV z component of velocity exceed the uncertainty analysis, and the cause of the discrepancy is not clear at this time. However, the SW-PDV and the CS-PDV z component of velocity were in excellent agreement with each other. This supports the argument that the difference between the PDV and LDV velocity results was systematic.

The instantaneous uncertainties increase to about 17% and 16% of the jet centerline velocity for both systems. Note that the largest uncertainty is in the y component of turbulence for the CS-PDV configuration and for the x component of the SW-PDV configuration. Recall that the y component of turbulence was noise dominated for the three-component CS-PDV setup. Theoretical investigations suggest that increased accuracy can be achieved by optimizing the combination of DSMS viewing directions.[14,17] The largest source of uncertainty was due to speckle noise. Speckle noise, among other factors, is dependent on the size of the seed particle that is used. The diameter of the condensed water and acetone particles used was estimated to be on the order of 50 nm. For the same incident laser wavelength and optical systems, the speckle noise will increase if larger particles are used.

Conclusion

PDV is a powerful nonintrusive optical diagnostic technique. As demonstrated, the technique can be configured to accurately measure three components of velocity in a planar measurement region. In developing the PDV technique, two different PDV systems were used to measure the velocity of a baseline flowfield. The SW-PDV system illuminated a streamwise plane, and the CS-PDV system illuminated a cross-stream plane. The flowfield from an ideally expanded Mach 2 axisymmetric jet exhausting into the ambient was the baseline flowfield. A set of LDV measurements was used as a reference measure of the mean velocity and turbulence level of this flowfield. Using this baseline flowfield and reference measurements, the accuracy of the PDV technique could be verified, and uncertainties in the technique could be investigated. A detailed uncertainty analysis of the PDV systems was also performed to properly evaluate them.

The mean velocities of the three-component SW-PDV system were in good agreement with the LDV results. Errors in the x component of mean velocity indicated that the method used to calculate the flatfield images needed to be improved. An improved method, which was found to be very reliable, was used in subsequent experiments. The SW-PDV turbulence measurements showed the same trend as the LDV turbulence measurements but were of slightly lower magnitude.

The three-component CS-PDV mean velocities were very good. However, due to speckle noise, the y component of turbulence intensity was noise dominated and the z component was significantly affected. Preliminary attempts to filter the images digitally to reduce the impact of the speckle noise were investigated.

A detailed uncertainty analysis was performed for both configurations. The uncertainty analysis indicated that the accuracy of the mean velocity was within 5% of the jet centerline velocity. The analysis also showed that the x component of the SW-PDV system and the y component of the CS-PDV system were most sensitive to noise. The accuracy of the PDV system was dependent on the specific configuration of the PDV system.

This paper has demonstrated the design and application of two different three-component PDV configurations. Each configuration elucidates different flow features. For example, shear layer growth characteristics can be studied using the SW-PDV system, whereas the CS-PDV system is excellent for investigating streamwise vorticity fields.[14]

Acknowledgments

The support of this research by the U.S. Air Force Office of Scientific Research, with L. Sakell and S. Walker as Technical Monitors, and by the NASA John H. Glenn Research Center at Lewis Field, with K. B. Zaman as Technical Monitor, is greatly appreciated. The assistance of D. J. Clancy in the preparation of the manuscript and in obtaining the experimental data is also greatly appreciated.

References

[1]Miles, R., Lempert, W., and Forkey, J., "Instantaneous Velocity Fields and Background Suppression by Filtered Rayleigh Scattering," AIAA Paper 91-0357, Jan. 1991.

[2]Forkey, J., Finkelstein, N., Lempert, W., and Miles, R., "Demonstration and Characterization of Filtered Rayleigh Scattering for Planar Velocity Measurements," *AIAA Journal*, Vol. 34, No. 3, 1996, pp. 442–448.

[3]Finkelstein, N. D., Lempert, W. R., and Miles, R. B., "Mercury Vapor Filter Technology and Ultraviolet Laser Source for Flowfield Imaging," AIAA Paper 97-0157, Jan. 1997.

[4]Yeh, Y., and Cummins, H., "Localized Fluid Flow Measurements with a He–Ne Laser Spectrometer," *Applied Physics Letters*, Vol. 4, No. 99, 1964, pp. 176–178.

[5]Komine, H., Brosnan, S., Litton, A. B., and Stappaerts, E. A., "Real-Time Doppler Global Velocimetry," AIAA Paper 91-0337, Jan. 1991.

[6]Meyers, J. F., Cavone, A. A., and Suzuki, K. E., "Investigation of the Vortical Flow Above an F/A-18 Using Doppler Global Velocimetry," *ASME Fifth International Conference on Laser-Anemometry—Advances and Applications*, Vol. 2, American Society of Mechanical Engineers, New York, 1993, pp. 1–16.

[7]Elliott, G. S., Samimy, M., and Arnette, S., "A Molecular Filter Based Velocimetry Technique for High Speed Flows," *Experiments in Fluids*, Vol. 18, No. 99, 1994, pp. 107–118.

[8]Arnette, S. A., Samimy, M., and Elliott, G. S., "Two-Component Filtered Planar Velocimetry in the Compressible Turbulent Boundary Layer," AIAA Paper 96-0305, Jan. 1996.

[9]Clancy, P. S., and Samimy, M., "Two-Component Planar Doppler Velocimetry in High-Speed Flows," *AIAA Journal*, Vol. 35, No. 11, 1997, pp. 1729–1738.

[10]Smith, M., Northam, G., and Drummond, J., "Application of Absorption Filter Planar Doppler Velocimetry to Sonic and Supersonic Jets," *AIAA Journal*, Vol. 34, No. 3, 1996, pp. 434–441.

[11]McKenzie, R., "Measurement Capabilities of Planar Doppler Velocimetry Using Pulsed Lasers," AIAA Paper 95-0297, Jan. 1995.

[12]McKenzie, R., "Planar Doppler Velocimetry Performance in Low-Speed Flows," AIAA Paper 97-0948, Jan. 1997.

[13]Clancy, P. S., Kim, J.-H., and Samimy, M., "Planar Doppler Velocimetry in High Speed Flows," AIAA Paper 96-1990, June 1996.

[14]Clancy, P., "Development and Application of Three-Component Planar Doppler Velocimetry for High Speed Flows," Ph.D. Dissertation, Dept. of Mechanical Engineering, Ohio State Univ., Columbus, OH, Dec. 1997.

[15]Elliott, G. S., Samimy, M., and Arnette, S. A., "Study of Compressible Mixing Layers Using Filtered Rayleigh Scattering Based Visualizations," *AIAA Journal*, Vol. 30, No. 10, 1992, pp. 2567–2569.

[16]Samimy, M., and Lele, S., "Motion of Particles with Inertia in a Compressible Shear Layer," *Physics of Fluids A*, Vol. 3, No. 99, 1991, pp. 1915–1923.

[17]Clancy, P. S., Samimy, M., and Erskine, W., "Planar Doppler Velocimetry: Three Component Velocimetry in Supersonic Jets," AIAA Paper 98-0506, Jan. 1998.

[18]Clancy, P. S., and Samimy, M., "Multiple-Component Velocimetry in High Speed Flows Using Planar Doppler Velocimetry," AIAA Paper 97-0497, Jan. 1997.

[19]Forkey, J. N., "Development and Demonstration of Filtered Rayleigh Scattering—A Laser Based Flow Diagnostic for Planar Measurement of Velocity, Temperature and Pressure," NASA Graduate Student Research, TR-NGT-50826, Princeton Univ., Princeton, NJ, April 1996.

[20]Wernet, M. P., "Stereo Viewing 3-Component, Planar PIV Utilizing Fuzzy Inference," AIAA Paper 96-2268, Jan. 1996.

[21]Fujii, H., and Asakura, T., "Effect of Surface Roughness on the Statistical Distribution of Image Speckle Intensity," *Optics Communications*, Vol. 11, No. 1, 1974, pp. 35–38.

[22]Fujii, H., and Asakura, T., "A Contrast Variation of Image Speckle Intensity Under Illumination of Partially Coherent Light," *Optics Communications*, Vol. 12, No. 1, 1974, pp. 32–38.

[23]Ohtsubo, J., and Asakura, T., "Measurement of Surface Roughness Properties Using Speckle Patterns with Non-Gaussian Statistics," *Optics Communications*, Vol. 25, No. 3, 1978, pp. 315–319.

[24]Arsenault, H. H., and April, G., "Properties of Speckle Integrated with a Finite Aperture and Logarithmically Transformed," *Journal of the Optical Society of America*, Vol. 66, No. 11, 1976, pp. 1160–1163.

[25]Dainty, J. C., "Introduction," *Topics in Applied Physics: Laser Speckle and Related Phenomena*, edited by J. C. Dainty, Vol. 9, Springer–Verlag, Berlin, 1984, pp. 1–7.

[26]Goodman, J. W., "Statistical Properties of Laser Speckle Patterns," *Topics in Applied Physics: Laser Speckle and Related Phenomena*, edited by J. C. Dainty, Vol. 9, Springer–Verlag, Berlin, 1984, pp. 9–75.

[27]Lim, J. S., "Image Restoration by Short Space Spectral Subtraction," *IEEE Transactions of Acoustics, Speech, and Signal Processing*, Vol. ASSP-28, No. 2, 1980, pp. 191–197.

[28]Lim, J. S., and Nawab, H., "Techniques for Speckle Noise Removal," *Applications of Speckle Phenomena*, edited by W. Carter, Vol. 243, Society of Photo-Optical Instrumentation Engineers, Spokane, WA, 1980, pp. 35–44.

[29]Jain, A. K., and Christensen, C. R., "Digital Processing of Images in Speckle Noise," *Applications of Speckle Phenomena*, edited by W. Carter, Vol. 243, Society of Photo-Optical Instrumentation Engineers, Spokane, WA, 1980, pp. 46–50.

[30]Kline, S. J., and McClintok, F. A., "Describing Uncertainties in Single Sample Experiments," *Mechanical Engineering*, Vol. 1, Jan. 1953, pp. 3–8.

[31]Moffat, R. J., "Describing the Uncertainties in Experimental Results," *Experimental Thermal and Fluid Sciences*, Vol. 1, 1988, pp. 3–17.

[32]Stark, H., and Woods, J. W., *Probability and Random Processes*, Prentice–Hall, Englewood Cliffs, NJ, 1994, Chap. 6.

R. P. Lucht
Associate Editor